CRYSTAL GROWTH & DESIGN

pubs.acs.org/crystal

Article

Crystallization, Phase Stability, and Electrochemical Performance of β-MoO_3 Thin Films

Øystein S. Fjellvåg,* Amund Ruud, Henrik H. Sønsteby, Ola Nilsen,* and Helmer Fjellvåg

Cite This: *Cryst. Growth Des.* 2020, 20, 3861−3866

Read Online

ACCESS | Metrics & More | Article Recommendations | Supporting Information

ABSTRACT: Insight into the crystallization process of functional materials deposited as thin films in an amorphous state is essential when phase pure samples of specific polymorphs are sought for utilization of performance aspects or fundamental studies. In this work, we report on controlled crystallization of α- and β-MoO_3 polymorphs from amorphous MoO_3 thin films produced by atomic layer deposition (ALD). The MoO_3 films are amorphous as deposited. Our experiments show that β-MoO_3 starts to crystallize from amorphous MoO_3 at a surprisingly low temperature of 185 °C, only 20 °C above the adopted ALD deposition temperature. Thin films of the β-MoO_3 polymorph start to slowly convert into α-MoO_3 at temperatures above 300 °C; however, long holding times are required to obtain phase pure products. High-quality thin film samples (electrodes) were characterized by electrochemical cycling toward lithium, demonstrating that α- and β-MoO_3 transfers into the same chemical state during cycling and that amorphous MoO_3 undergoes less change upon cycling.

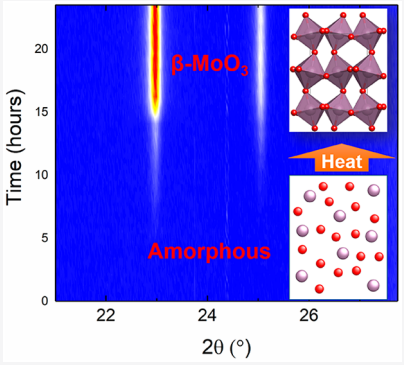

1. INTRODUCTION

The atomic arrangements of solid materials strongly influence their functional properties. This is especially important in cases where the crystal growth procedures of functional materials can result in different polymorphs. Reliable synthesis routes for phase pure samples are highly valued, particularly as a basis for detailed physicochemical characterizations. When achievable, amorphous (noncrystalline/nano) materials are good starting points for the formation of phase pure materials of specific polymorphs through controlled crystallization. In this paper, we investigate the conversion of X-ray amorphous molybdenum trioxide (MoO_3) into the α- and β-MoO_3 polymorphs with the aim of achieving phase pure samples.

MoO_3 has shown great potential within the fields of catalysis,[1−3] optical devices,[4] memory devices,[5] gas sensing technologies,[6] and electrochromism,[7] and exists in several polymorphic forms. In addition to the stable α-MoO_3 polymorph, metastable β-MoO_3 (Figure 1), ε-, γ-, and h-MoO_3 are reported.[8−15] α-MoO_3 adopts a layered orthorhombic structure constructed of ABAB... stacked bilayers of distorted MoO_6-octahedra that interact via van der Waals interactions.[8,16] Metastable β-MoO_3 is formed via crystallization of amorphous MoO_3 under careful annealing.[9,17] β-MoO_3 adopts the WO_3-structure type, a distorted ReO_3-type structure, and can be described as a perovskite (ABO_3) with an empty A-site. Conversion of β-MoO_3 into the stable α-MoO_3 can be achieved by heating above 350 °C.[14,18]

For applications in electrochemical devices, α-MoO_3 has been for more than 30 years considered a potential cathode for lithium-ion batteries, due to its high theoretical capacity (372 mAh g^{-1}) when a two-electron reaction is exploited; 2Li + $MoO_3 \leftrightarrow Li_2MoO_3$.[19,20] However, it is challenged by a reduced Coulombic efficiency after prolonged cycling. Nanochemical methods, exploiting nanoscopic morphologies (i.e., nanobelts) and/or doping with, e.g., nitrogen, have improved the Coulombic efficiency, and state-of-the-art specific capacity values are ~250 mAh g^{-1} after 300 cycles.[21,22] The two-electron reaction occurs at moderately high potentials versus Li/Li^+, making α-MoO_3 suitable in devices demanding high energy density. The electrochemical performance of the β-

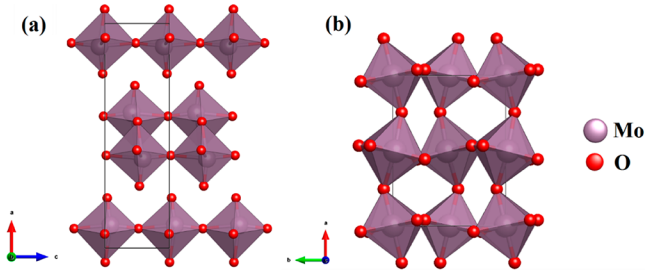

Figure 1. Crystal structure of (a) α-MoO_3 (*Pnma*) and (b) β-MoO_3 ($P12_1/c1$).[8,13] α-MoO_3 takes a layered structure based on stacked bilayers, while β-MoO_3 adopts the WO_3 type structure, corresponding to the perovskite structure with empty A-sites.

Received: February 6, 2020
Revised: April 28, 2020
Published: April 28, 2020

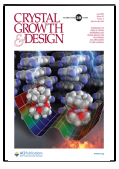

MoO_3 polymorph is not widely studied, but its properties are hypothesized to be similar to α-MoO_3.[23,24] The limited interest in β-MoO_3 is possibly related to difficulties in synthesizing phase pure samples.[23]

Various polymorphs of MoO_3 have previously been deposited as thin films by several techniques, including pulsed laser deposition,[25] molecular beam epitaxy,[26] chemical vapor deposition,[27] RF sputtering,[28] and atomic layer deposition (ALD).[17] The current focus is on the latter ALD technique in which amorphous films are obtained at the relatively low deposition temperature of 165 °C.[29] Diskus et al. prepared amorphous MoO_3 by ALD and crystallized these films into both β- and α-MoO_3 by thermal post-treatment.[17] The β-MoO_3 phase was obtained by annealing for 12 min at 500 °C on Si(111) or 8 min at 400 °C on Al_2O_3(001), although α-MoO_3 impurities were observed.[17,30] In the current work, we revisit the postdeposition crystallization process using *in situ* diffraction, with the aim of achieving phase pure thin films of β- and α-MoO_3. Finally, we evaluate the electrochemical performance of β- and α-MoO_3 thin films in lithium-ion batteries.

2. EXPERIMENTAL SECTION

Amorphous MoO_3 thin films were deposited in an F-120 Sat (ASM Microchemistry Ltd.) reactor at 165 °C based on the work by Diskus et al. using water, ozone, and molybdenum carbonyl ($Mo(CO)_6$, (Sigma-Aldrich)) as precursors.[17] The overall reaction is based on sequential exposure of the surface with vapor of $Mo(CO)_6$ and a combination of ozone and water. The process is highly temperature sensitive outside the temperature range 157−173 °C, inside which a growth rate of 0.7 Å/cycle is obtained. More details on the process and its ALD nature is given in ref 17. In the hot-wall, cross-flow reactor, the precursors were pulsed by inert gas valves into the reaction chamber.[31] The reactor pressure during deposition was on the order of 1 mbar. Water and molybdenum carbonyl precursors were kept at room temperature as this yield sufficient vapor pressure. Nitrogen was pulsed over the molybdenum carbonyl precursor as a carrier gas to help transport the precursor into the reactor. Ozone was generated from 99.6% O_2 (AGA) by a BMT 803N ozone generator, giving an ozone concentration of ∼15 wt % O_3 in O_2. Film thickness was analyzed by spectroscopic ellipsometry (J. A. Woollam α-SE) for a wavelength range of 380−900 nm. The thin film samples used for crystallization studies had a thickness of ∼100 nm, deposited on Si(100) substrates. Rapid heat treatment (<1 h) was carried out in a rapid thermal processing (RTP) furnace (OTF-1200X-4-RTP-UL, (MTI Corp.)) in 1 atm air. Longer heat treatments (>1 h) were carried out in a standard tube furnace in 1 atm air.

X-ray diffraction (XRD) data were collected on a Bruker AXS D8 powder diffractometer equipped with a Cu tube, a Ge(111) monochromator, and a LynxEye detector. *In situ* diffraction data were collected on a PANalytical Empyrean diffractometer with a parallel beam mirror and a 1/32° divergence slit. Static XRD patterns were collected with a PIXcel3D detector equipped with a 0.04° rad soller slit, in static line mode and scanned in the 2θ-range from 21.00 to 27.75°. *In situ* annealing was carried out with an Anton Paar DHS 1100 stage under an air cooled carbon dome in air.

Coin cells (CR2032) were assembled in a glovebox (MBraun) with O_2 and H_2O levels <0.1 ppm under an argon atmosphere (AGA, 99.999%). The working electrode, 100 nm of MoO_3 deposited on a 316 stainless steel disk, was separated from the Li metal counter electrode by electrolyte-soaked glass fiber separator (GF/C, Whatman). A 1.0 M solution of $LiClO_4$ (99.99%, Aldrich) in ethylene carbonate/dimethyl carbonate (EC/DMC 1:1 in volume, 99% Sigma-Aldrich) was used as electrolyte. Cyclic voltammetry (CV) measurements were carried out in the potential range of 1.0−4.0 V vs Li/Li^+ at a sweep rate of 0.1 mV s^{-1} with an MPG-2 battery tester (BioLogic).

3. RESULTS AND DISCUSSION

The MoO_3 thin films were amorphous as-deposited, consistent with previous reports.[17,30] The initial approach for crystallization of the samples was to anneal the films at 300 and 500 °C for 10 min in an RTP furnace, resulting in predominantly β-MoO_3 at 300 °C and α-MoO_3 at 500 °C, respectively (Figure 2). Although crystalline β-MoO_3 dominates after annealing at

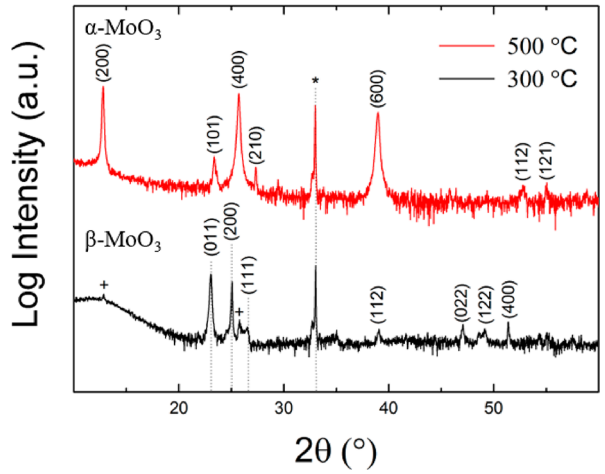

Figure 2. Diffraction patterns of initially amorphous MoO_3 films after annealing for 10 min shows the presence of α-MoO_3 (*Pnma*) at 500 °C and of β-MoO_3 ($P12_1/c1$) at 300 °C, red and black patterns, respectively. Weak signatures of (200) and (400) from the α-MoO_3 phase are present in the sample annealed at 300 °C, as marked by +; (200) from the Si substrate is marked by *.

300 °C, the presence of (200) and (400) of the α-MoO_3 phase is apparent.[9,17] Contrary to previous reports, we do not observe any presence of the β-MoO_3 phase for samples annealed at 500 °C. Note that the α-MoO_3 films appear as highly oriented in the [100] direction with (h00) Bragg reflections dominating the diffraction pattern, possibly due to heterogeneous nucleation and columnar growth during annealing.

A primary challenge is the formation of phase pure β-MoO_3 thin films, owing to its metastable nature. Hence, the appropriate conditions for nucleating β-MoO_3 from the amorphous deposit without formation of the thermodynamically stable α-MoO_3 phase requires a delicate balance in temperature and time that was not achieved in our initial *ex situ* annealing attempt (Figure 2).[32] We therefore address this phase transformation issue utilizing *in situ* temperature variable diffraction crystallization experiments.

Initial *in situ* heating experiments with slow ramping of the annealing temperature show that β-MoO_3 crystallizes at lower temperatures than earlier anticipated, i.e., already below 200 °C. Therefore, we set the starting temperature of the *in situ* heating experiment at 180 °C, slightly above the adopted deposition temperature of 165 °C. This temperature was held for 3.25 h while diffraction patterns were collected regularly (every ∼30 min). After 3.25 h at 180 °C, no signs of crystallization were observed (Figure 3). We therefore conclude that the amorphous as-grown phase is kinetically stable at the deposition temperature for all practical concerns.

The heating sequence (isothermal for 3.25 h followed by dynamic steps of 5 °C) was continued up to 210 °C. After 2.8 h at 185 °C, the (011)-reflection of β-MoO_3 emerges, as

https://dx.doi.org/10.1021/acs.cgd.0c00156
Cryst. Growth Des. 2020, 20, 3861−3866

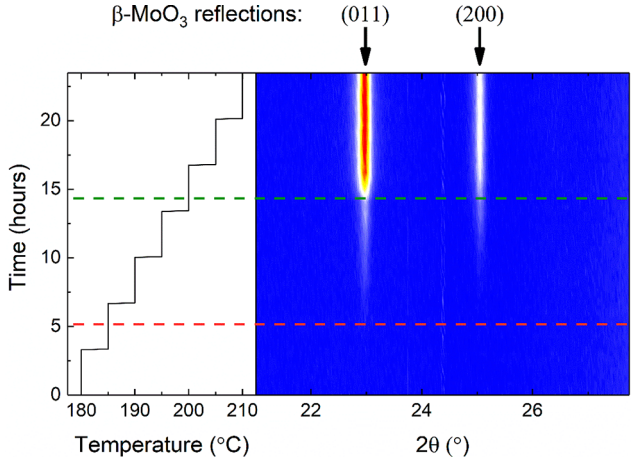

Figure 3. *In situ* crystallization diffraction experiment of amorphous MoO_3 thin films on Si(100). Left: Temperature profile of the experiment. Right: Contour plot of the collected diffraction patterns. The (011)- and (200)-reflections of β-MoO_3 are marked. The red and green dashed lines indicate the first signs of crystallization and point of increased crystal growth, respectively.

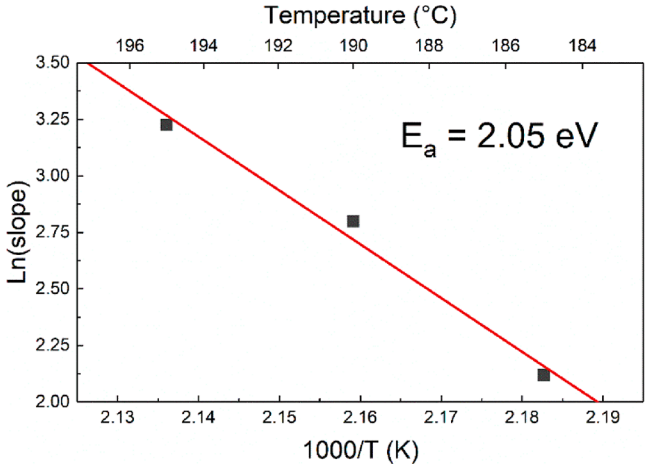

Figure 4. Arrhenius plot for slopes extracted from XRD crystallization experiments (black squares) and linear fit (red line). The activation energy for nucleation of β-MoO_3 is calculated to 2.05 eV.

marked by the dashed red line in Figure 3. The intensity of (011) continues to increase slowly up to 200 °C, indicating continued nucleation of β-MoO_3. During the isothermal step at 200 °C, the intensity of (011) rapidly increases, as marked by the dashed green line in Figure 3, indicating an onset of crystal growth. Above 200 °C, the intensity of (011) remains constant. No further change was observed in the diffraction pattern upon subsequent cooling.

The observed variation in diffracted intensities indicates at least two kinetically limited processes. It is natural to assume these are nucleation and growth, respectively, as already indicated above. The driving force for nucleation dominates at lower temperatures, while higher temperatures govern the required diffusion process for growth. Assuming this to be directly transferrable to our case, we conclude on continuous nucleation of β-MoO_3 up to 200 °C whereafter rapid crystal growth takes over. By applying an Arrhenius law for extracted increments in the diffracted intensity of (110) for β-MoO_3 as a function of temperature (Figure S1, Supporting Information), we deduce an activation energy for nucleation of β-MoO_3 in amorphous MoO_3 of 2.05 eV (Figure 4). Our identification of an activation energy for nucleation illustrates well the notable differences in phase formation during annealing between our study and the one by Diskus et al.[17] Diskus shows a transition from β-MoO_3 to α-MoO_3 within 10−15 min for annealing at 500 °C, while we observe a similar transition at 340 °C after some hours. This is according to a temperature−time-transition.[33]

We note that the crystallization temperature of amorphous MoO_3 into β-MoO_3 at 185 °C occurs close to the ALD deposition temperature of 165 °C. One may therefore speculate whether deposition at higher temperatures would yield crystalline β-MoO_3 phase directly. However, the deposition temperature window is limited upward by the thermal stability of the $Mo(CO)_6$-precursor and depositions at higher temperatures were therefore not attempted.[17] We note that alternative precursors allow deposition of MoO_3 at higher temperatures; however, β-MoO_3 is not reported to be obtained as deposited by ALD, only in mixture with other phases.[34−36] On the other hand, on the basis of the similarity in crystal structure and unit cell parameters between β-MoO_3 and perovskite-type oxides such as $SrTiO_3$ and $LaAlO_3$, we hypothesize that deposition on such single-crystal perovskite substrates can stabilize the β-MoO_3 phase at 165 °C. This represents opportunities for future studies.

β-MoO_3 (ρ = 4.50 g·cm^{-3}) has a more open structure than α-MoO_3 (ρ = 4.75 g·cm^{-3}) with corner-shared octahedra compared to edge-sharing octahedral bilayers and is thus expected to nucleate first if allowed enough time.[8,13] Nevertheless, the onset temperature for nucleation of α-MoO_3 is a very relevant parameter for ensuring conditions that might yield phase pure β-MoO_3. From our initial experiments, we know that α-MoO_3 nucleate at 300 °C (Figure 2). Further, *in situ* diffraction experiments in the temperature range 200−310 °C, with isothermal annealing for 50 min after each 5 °C (dynamic) temperature step, showed no sign of α-MoO_3 formation This is contrary to our observation of coexistence of the α- and β-MoO_3 after annealing at 300 °C (Figure 2), suggesting that nucleation of α-MoO_3 is also kinetically hindered. We ascribe this contradiction to the difference between an RTP and a conventional furnace. In an RTP, the sample is heated by absorption of light, and the temperature is reached extremely fast, while in conventional furnaces that have a large thermal mass, more time may be needed for a sample to reach thermal equilibrium. In addition, a slight deviation in calibration may be the origin of the contradictory result.

This hypothesis was investigated by long-term annealing at selected temperatures. Amorphous films of MoO_3 were annealed at 235 °C for 1 and 10 days, respectively, and at 250 °C for 1 h. Evaluation by XRD after annealing shows that all films consist of phase pure β-MoO_3, with no sign of α-MoO_3 (Figure 5). Evidently, these temperatures are sufficiently low to suppress the nucleation of α-MoO_3. Therefore, we suggest that phase pure films of β-MoO_3 can be obtained by annealing in the temperature range 200−250 °C and that long annealing times are ideal due to slow nucleation and crystal growth. The low crystallization temperatures of β-MoO_3 are of great interest since they allow for monolithic integration in silicon-based electronic devices (integrated circuits) at low thermal budgets, for example, electrochromic applications.

We further investigated the transition from β-MoO_3 to α-MoO_3 by carrying out an isothermal experiment at 340 °C on a

https://dx.doi.org/10.1021/acs.cgd.0c00156
Cryst. Growth Des. 2020, 20, 3861−3866

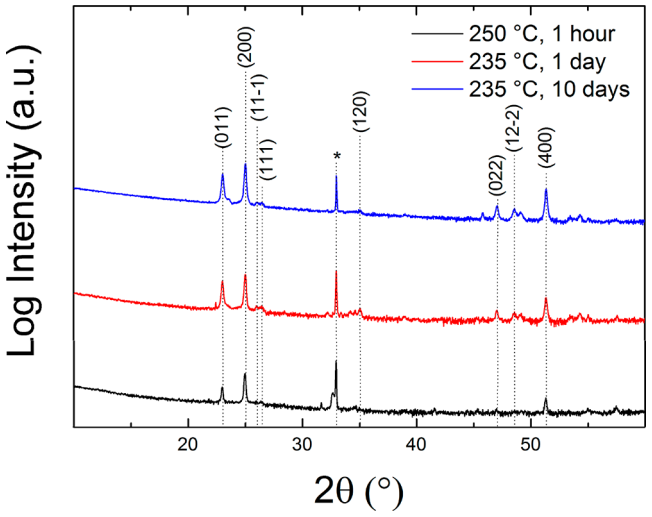

Figure 5. XRD patterns of β-MoO_3 thin films realized by annealing at 250 °C for 1 h in an RTP furnace (black) and at 235 °C for 1 (red) and 10 (blue) days in a tube furnace. The reflections are indexed according to β-MoO_3 ($P12_1/c1$). * marks (200) from the Si substrate.

sample of β-MoO_3 prepared by heating at 250 °C for 1 h (Figure 6). α-MoO_3 appears after 1 h at 340 °C. We clearly observe the reflections from both the α- and β-MoO_3 phases throughout the conversion of the β-MoO_3 film into α-MoO_3. The two phases coexist during the transformation process, which represent a reconstructive first-order phase transition where α-MoO_3 nucleates from the matrix of β-MoO_3. The presence of β-MoO_3, even after 6 h (total duration of the experiment), suggests that the nucleation of α-MoO_3 is a limiting factor for the phase conversion. The α-modification is maintained upon cooling, pointing toward an irreversible transformation from β- to α-MoO_3.

The electrochemical performance of β-MoO_3 is poorly explored and calls for attention. Cyclic voltammetry (CV) studies were therefore performed for the β-MoO_3 thin films in

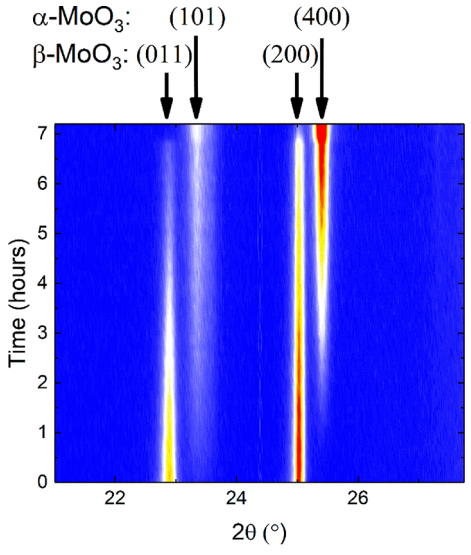

Figure 6. Contour plot of the diffraction patterns collected during an isothermal *in situ* diffraction experiment at 340 °C, displaying the conversion from the β- into the α-MoO_3 phase. Reflections originating from α- and β-MoO_3 are marked with Miller indices.

the potential range 1.00−4.00 V vs Li/Li^+ (Figure 7). The crystalline sample annealed for 24 h at 235 °C displays two irreversible cathodic reactions at 2.60 and 1.57 V during the first discharge (Figure 7a). A first cycle anodic peak is observed at about 2.70 V during charging. We observe a large cathodic peak at about 2.21 V, and an anodic peak at about 2.43 V, in the second and 10th cycle. However, the peak positions shift somewhat from the second to the 10th cycle, toward a higher potential for the cathodic reaction, and toward a lower potential for the anodic reaction, meaning a reduction in overpotential for the involved redox pair. In addition, very broad cathodic and anodic peaks emerge for the 10th cycle at 3.30/3.50 V, indicating an electrochemically induced redox reaction. The reversible redox pair (2.21/2.43 V) is in line with previously reported values for α-MoO_3, indicating the reaction:[19,20]

$$MoO_3 + xLi \leftrightarrow Li_xMoO_3\ (0 < x < \sim 1.5)$$

From the second cycle, the electrochemical behavior of α- and β-MoO_3 is very similar, i.e., the redox potentials are similar, and the overall shape of the CV-curves are similar. We believe this suggests that both compounds gradually transform into the same state upon cycling. However, this is beyond the scope of this work and is left for future studies.

In comparison, the sample annealed for 1 h at 250 °C shows significantly less defined electrochemical reactions. Cathodic reactions at 2.34 and 1.55 V are present; however, they appear reversible and weaker compared to the sample annealed for 24 h at 235 °C (Figure 7b). We ascribe the difference in electrochemical performances of the two samples to a difference in crystallinity. For well-defined and crystalline materials, we expect redox reactions within relatively well-defined potential ranges, as observed for the sample heated at 235 °C for 24 h. This is in contrast to the sample heated at 250 °C for 1 h, which reflects mostly an amorphous state. This result indicates that 1 h of annealing at 250 °C is insufficient for complete conversion of the amorphous material.

The electrochemical reactions in β-MoO_3 occur at a higher potential in the first cycle than reported for α-MoO_3 in the literature. This indicates a more ionic Mo−O bonding in β-MoO_3, in compliance with the structures (Figure 1) where the polyhedra in β-MoO_3 are corner-shared, whereas the connectivity of the octahedra in α-MoO_3 include edge-sharing. Furthermore, the state that β-MoO_3 and α-MoO_3 is transformed into upon cycling appears to be more covalent than the starting oxides. Amorphous MoO_3, on the other hand, behaves differently from both α- and β-MoO_3, and undergoes less change upon cycling, although with less defined electrochemical reactions (Figure 7b).

Our current findings raise questions on the amorphous phase fraction in the β-MoO_3 samples electrochemically investigated in this and other works. The electrochemical data for the sample heated at 235 °C for 24 h are well in line with a complete crystallization into β-MoO_3. On the other hand, the sample heated at 250 °C for 1 h still contains large mass fractions of amorphous MoO_3 that cannot be detected by XRD. We therefore speculate whether some of the attractive properties reported for β-MoO_3 for lithium-ion batteries may emerge from the remains of amorphous MoO_3, withstanding a larger number of cycles before deterioration. Amorphous materials often display high performance in electrochemical devices, e.g., the ultrahigh power capabilities shown for amorphous iron phosphate.[37]

https://dx.doi.org/10.1021/acs.cgd.0c00156
Cryst. Growth Des. 2020, 20, 3861−3866

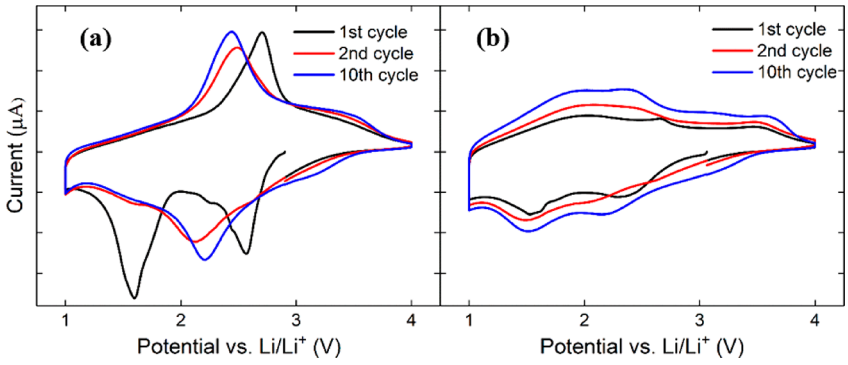

Figure 7. CV measurements between 1.0 and 4.0 V for 100 nm β-MoO_3 films deposited on steel substrates and annealed at (a) 235 °C for 24 h and (b) 250 °C for 1 h.

4. CONCLUSION

In summary, we have investigated the crystallization process of amorphous MoO_3 thin films deposited by ALD into α- and β-MoO_3 upon heating. We find that β-MoO_3 nucleates from amorphous MoO_3 during isothermal annealing at 185 °C. Phase pure films of β-MoO_3 are prepared by prolonged annealing between 235 and 250 °C. Nucleation of α-MoO_3 initiates at ∼300 °C, and temperatures above 340 °C are suitable for crystallization into phase pure samples. Quite long annealing times are needed due to slow nucleation of α-MoO_3 at low temperatures. The electrochemical evaluation of β-MoO_3 as a cathode material for thin-film lithium-ion batteries signified the importance of long annealing times to achieve good crystallinity and quality of the thin-film electrodes. However, crystalline β-MoO_3 is seemingly transferred into the same lithiated electrochemical state as α-MoO_3 during cycling. Amorphous MoO_3 shows increased cycling stability, although with less defined electrochemical features. Both α- and β-MoO_3 can successfully be crystallized at relatively low temperatures, opening for monolithic integration in electronic devices where thermal budget is of concern, such as silicon-based electronics.

■ ASSOCIATED CONTENT

Supporting Information

The Supporting Information is available free of charge at https://pubs.acs.org/doi/10.1021/acs.cgd.0c00156.

Figure displaying the increments in the diffracted intensity of the (110) reflection of β-MoO_3 for the different temperature regions in the *in situ* heating experiment (Figure S1) (PDF)

■ AUTHOR INFORMATION

Corresponding Authors

Øystein S. Fjellvåg − *Centre for Materials Science and Nanotechnology, Department of Chemistry, University of Oslo, N-0315 Oslo, Norway; Department for Neutron Materials Characterization, Institute for Energy Technology, NO-2027 Kjeller, Norway;* orcid.org/0000-0003-0215-5260; Email: o.s.fjellvag@smn.uio.no, oystein.fjellvag@ife.no

Ola Nilsen − *Centre for Materials Science and Nanotechnology, Department of Chemistry, University of Oslo, N-0315 Oslo, Norway;* orcid.org/0000-0002-2824-9153; Email: ola.nilsen@uio.no

Authors

Amund Ruud − *Centre for Materials Science and Nanotechnology, Department of Chemistry, University of Oslo, N-0315 Oslo, Norway;* orcid.org/0000-0002-8752-3044

Henrik H. Sønsteby − *Centre for Materials Science and Nanotechnology, Department of Chemistry, University of Oslo, N-0315 Oslo, Norway;* orcid.org/0000-0002-5597-1125

Helmer Fjellvåg − *Centre for Materials Science and Nanotechnology, Department of Chemistry, University of Oslo, N-0315 Oslo, Norway;* orcid.org/0000-0001-6045-7211

Complete contact information is available at: https://pubs.acs.org/10.1021/acs.cgd.0c00156

Funding

This work was partially performed within the RIDSEM project, financed in full by the Research Council of Norway (Project No. 272253).

Notes

The authors declare no competing financial interest.

■ ACKNOWLEDGMENTS

The authors gratefully acknowledge the use of the Norwegian Center for X-ray Diffraction, Scattering and Imaging (RECX).

■ REFERENCES

(1) Larrubia, M. A.; Ramis, G.; Busca, G. An FT-IR study of the adsorption of urea and ammonia over V_2O_5−MoO_3−TiO_2 SCR catalysts. *Appl. Catal., B* **2000**, *27*, L145−L151.

(2) Ferroni, M.; Guidi, V.; Martinelli, G.; Sacerdoti, M.; Nelli, P.; Sberveglieri, G. MoO_3-based sputtered thin films for fast NO_2 detection. *Sens. Actuators, B* **1998**, *48*, 285−288.

(3) Sunu, S. S.; Prabhu, E.; Jayaraman, V.; Gnanasekar, K. I.; Gnanasekaran, T. Gas sensing properties of PLD made MoO_3 films. *Sens. Actuators, B* **2003**, *94*, 189−196.

(4) Wang, L.; Lv, Y.; Lin, J.; Fan, Y.; Zhao, J.; Wang, Y.; Liu, X. High-efficiency inverted quantum dot light-emitting diodes with enhanced hole injection. *Nanoscale* **2017**, *9*, 6748−6754.

(5) Abhijith, T.; Kumar, T. V. A.; Reddy, V. S. Organic bistable memory devices based on MoO_3 nanoparticle embedded Alq_3 structures. *Nanotechnology* **2017**, *28*, 095203.

(6) Alsaif, M. M. Y. A.; Balendhran, S.; Field, M. R.; Latham, K.; Wlodarski, W.; Ou, J. Z.; Kalantar-Zadeh, K. Two dimensional α-MoO_3 nanoflakes obtained using solvent-assisted grinding and sonication method: Application for H_2 gas sensing. *Sens. Actuators, B* **2014**, *192*, 196−204.

(7) Prasad, A. K.; Gouma, P. I. MoO_3 and WO_3 based thin film conductimetric sensors for automotive applications. *J. Mater. Sci.* **2003**, *38*, 4347−4352.

(8) Negishi, H.; Negishi, S.; Kuroiwa, Y.; Sato, N.; Aoyagi, S. Anisotropic thermal expansion of layered MoO_3 crystals. *Phys. Rev. B: Condens. Matter Mater. Phys.* **2004**, *69*, 064111.
(9) McCarron, E. M. β-MoO_3: a metastable analogue of WO_3. *J. Chem. Soc., Chem. Commun.* **1986**, 336−338.
(10) McCarron, E. M.; Calabrese, J. C. The growth and single crystal structure of a high pressure phase of molybdenum trioxide: MoO_3-II. *J. Solid State Chem.* **1991**, *91*, 121−125.
(11) Zheng, L.; Xu, Y.; Jin, D.; Xie, Y. Novel Metastable Hexagonal MoO_3 Nanobelts: Synthesis, Photochromic, and Electrochromic Properties. *Chem. Mater.* **2009**, *21*, 5681−5690.
(12) Olenkova, I. P.; Plyasova, L. M.; Kirik, S. D. Crystal structure of "hexagonal" MoO_3. *React. Kinet. Catal. Lett.* **1981**, *16*, 81−85.
(13) Parise, J. B.; McCarron, E. M.; Von Dreele, R.; Goldstone, J. A. β-MoO_3 produced from a novel freeze drying route. *J. Solid State Chem.* **1991**, *93*, 193−201.
(14) de Castro, I. A.; Datta, R. S.; Ou, J. Z.; Castellanos-Gomez, A.; Sriram, S.; Daeneke, T.; Kalantar-Zadeh, K. Molybdenum Oxides − From Fundamentals to Functionality. *Adv. Mater.* **2017**, *29*, 1701619.
(15) Slawinski, W. A.; Fjellvåg, Ø. S.; Ruud, A.; Fjellvåg, H. A novel polytype - the stacking fault based γ-MoO_3 nanobelts. *Acta Crystallogr., Sect. B: Struct. Sci., Cryst. Eng. Mater.* **2016**, *72*, 201−208.
(16) Ma, W.; Alonso-González, P.; Li, S.; Nikitin, A. Y.; Yuan, J.; Martín-Sánchez, J.; Taboada-Gutiérrez, J.; Amenabar, I.; Li, P.; Vélez, S.; Tollan, C.; Dai, Z.; Zhang, Y.; Sriram, S.; Kalantar-Zadeh, K.; Lee, S.-T.; Hillenbrand, R.; Bao, Q. In-plane anisotropic and ultra-low-loss polaritons in a natural van der Waals crystal. *Nature* **2018**, *562*, 557−562.
(17) Diskus, M.; Nilsen, O.; Fjellvåg, H. Growth of thin films of molybdenum oxide by atomic layer deposition. *J. Mater. Chem.* **2011**, *21*, 705−710.
(18) Carcia, P. F.; McCarron, E. M. Synthesis and properties of thin film polymorphs of molybdenum trioxide. *Thin Solid Films* **1987**, *155*, 53−63.
(19) Besenhard, J. O.; Heydecke, J.; Fritz, H. P. Characteristics of molybdenum oxide and chromium oxide cathodes in primary and secondary organic electrolyte lithium batteries I. Morphology, structure and their changes during discharge and cycling. *Solid State Ionics* **1982**, *6*, 215−224.
(20) Besenhard, J. O.; Heydecke, J.; Wudy, E.; Fritz, H. P.; Foag, W. Characteristics of molybdenum oxide and chromium oxide cathodes in primary and secondary organic electrolyte lithium batteries. Part II. Transport properties. *Solid State Ionics* **1983**, *8*, 61−71.
(21) Wang, X.-J.; Nesper, R.; Villevieille, C.; Novák, P. Ammonolyzed MoO_3 Nanobelts as Novel Cathode Material of Rechargeable Li-Ion Batteries. *Adv. Energy Mater.* **2013**, *3*, 606−614.
(22) Zhou, L.; Yang, L.; Yuan, P.; Zou, J.; Wu, Y.; Yu, C. α-MoO3 Nanobelts: A High Performance Cathode Material for Lithium Ion Batteries. *J. Phys. Chem. C* **2010**, *114*, 21868−21872.
(23) Juárez Ramírez, I.; Martínez-de la Cruz, A. Synthesis of β-MoO3 by vacuum drying and its structural and electrochemical characterisation. *Mater. Lett.* **2003**, *57*, 1034−1039.
(24) Mariotti, D.; Lindström, H.; Bose, A. C.; Ostrikov, K. Monoclinic β-MoO_3 nanosheets produced by atmospheric micro-plasma: application to lithium-ion batteries. *Nanotechnology* **2008**, *19*, 495302.
(25) Ramana, C. V.; Atuchin, V. V.; Pokrovsky, L. D.; Becker, U.; Julien, C. M. Structure and chemical properties of molybdenum oxide thin films. *J. Vac. Sci. Technol., A* **2007**, *25*, 1166−1171.
(26) Altman, E. I.; Droubay, T.; Chambers, S. A. Growth of MoO_3 films by oxygen plasma assisted molecular beam epitaxy. *Thin Solid Films* **2002**, *414*, 205−215.
(27) Ivanova, T.; Gesheva, K.; Hamelmann, F. Morphological and structural study of CVD MoO_3-Cr_2O_3 films. *ECS Trans.* **2009**, *25*, 221−228.
(28) Yordanov, R.; Boyadjiev, S.; Georgieva, V.; Vergov, L. In Characterization of thin MoO_3 films formed by RF and DC-magnetron reactive sputtering for gas sensor applications. *J. Phys.: Conf. Ser.*; IOP Publishing: 2014; p 012040.
(29) Sønsteby, H. H.; Fjellvåg, H.; Nilsen, O. Functional Perovskites by Atomic Layer Deposition − An Overview. *Adv. Mater. Interfaces* **2017**, *4*, 1600903.
(30) Diskus, M.; Nilsen, O.; Fjellvag, H.; Diplas, S.; Beato, P.; Harvey, C.; van Schrojenstein Lantman, E.; Weckhuysen, B. M. Combination of characterization techniques for atomic layer deposition MoO_3 coatings: From the amorphous to the orthorhombic α-MoO_3 crystalline phase. *J. Vac. Sci. Technol., A* **2012**, *30*, 01A107.
(31) Suntola, T. Atomic layer epitaxy. *Thin Solid Films* **1992**, *216*, 84−89.
(32) Pham, T. T. P.; Nguyen, P. H. D.; Vo, T. T.; Nguyen, H. H. P.; Luu, C. L. Facile method for synthesis of nanosized β−MoO_3 and their catalytic behavior for selective oxidation of methanol to formaldehyde. *Adv. Nat. Sci.: Nanosci. Nanotechnol.* **2015**, *6*, 045010.
(33) Lu, K.; Lück, R.; Predel, B. The temperature vs time transformation (T-T-T) diagram for a transition from the amorphous to the nanocrystalline state. *Acta Metall. Mater.* **1994**, *42*, 2303−2311.
(34) Mattinen, M.; Wree, J.-L.; Stegmann, N.; Ciftyurek, E.; Achhab, M. E.; King, P. J.; Mizohata, K.; Räisänen, J.; Schierbaum, K. D.; Devi, A.; Ritala, M.; Leskelä, M. Atomic Layer Deposition of Molybdenum and Tungsten Oxide Thin Films Using Heteroleptic Imido-Amidinato Precursors: Process Development, Film Characterization, and Gas Sensing Properties. *Chem. Mater.* **2018**, *30*, 8690−8701.
(35) Mattinen, M.; King, P. J.; Khriachtchev, L.; Heikkilä, M. J.; Fleming, B.; Rushworth, S.; Mizohata, K.; Meinander, K.; Räisänen, J.; Ritala, M.; Leskelä, M. Atomic layer deposition of crystalline molybdenum oxide thin films and phase control by post-deposition annealing. *Mater. Today Chem.* **2018**, *9*, 17−27.
(36) Vos, M. F. J.; Macco, B.; Thissen, N. F. W.; Bol, A. A.; Kessels, W. M. M. Atomic layer deposition of molybdenum oxide from $(NtBu)_2(NMe_2)_2Mo$ and O_2 plasma. *J. Vac. Sci. Technol., A* **2016**, *34*, 01A103.
(37) Gandrud, K. B.; Nilsen, O.; Fjellvåg, H. Ultra-high power capabilities in amorphous $FePO_4$ thin films. *J. Power Sources* **2016**, *306*, 454−458.

https://dx.doi.org/10.1021/acs.cgd.0c00156
Cryst. Growth Des. 2020, 20, 3861−3866